Time-Modulated Array Beamforming with Periodic Stair-Step Pulses

Roberto Maneiro-Catoira, Julio Brégains, José A. García-Naya[1,*], Luis Castedo[1]

Universidade da Coruña (University of A Coruña), CITIC Research Center
Campus de Elviña s/n, 15071 A Coruña, Spain

Abstract

Time-modulated arrays (TMAs) are able to improve the side-lobe level of the radiation pattern at the fundamental mode but cannot steer the beam at such a mode towards a given direction. Beam-steering is possible in a TMA, but only at the harmonic patterns and at the expense of a severe TMA efficiency reduction. In this work we propose a TMA approach that simultaneously performs both features over the same beam by using two sets of switches: (1) single-pole four-throw switches to generate periodic stair-step pulses suitable for efficiently synthesizing a uniform steerable beam over the first positive harmonic, and (2) single-pole single-throw switches to reconfigure the side-lobe level of the previous beam. Performance, small size, cost-effectiveness, and performance invariability with the carrier frequency are features that make this TMA approach a competitive solution for analog beamforming. Accordingly, the structure is an attractive proposal for the design of multibeam transceivers.

Keywords: antenna arrays, time-modulated arrays, antenna efficiency, beam steering.

1. Introduction

Hybrid digital-analog beamforming architectures reduce hardware cost and avoid the high energy consumption exhibited by fully digital solutions [14, 16, 27]. Nevertheless, since the analog part in these hybrid solutions is in general based on variable phase shifters (VPSs), there is still room for further improvement not only in terms of cost, but also in terms of phase resolution and insertion losses [7]. Switched time-modulated arrays (TMAs) [20] constitute an interesting alternative to VPS-based analog beamforming networks (BFNs).

Although the theoretical basis of the beam-steering capabilities of TMAs was stated by the pioneering work in [31], it is not until the arrival of systematic optimization algorithms when TMA beam-steering design is addressed with renewed vigor [17, 32]. TMA adaptive beamforming was originally studied in [18] considering the radiation patterns at the fundamental mode (static) and at the first harmonics (steerable). Subsequent works address the TMA harmonic beamforming by focusing on the mitigation of interfering signals [29] and on the exploitation of a key differential feature of TMAs: the exchange of spatial and frequency diversity [23, 24, 28, 30, 33].

A common denominator among all the previous works is that the efficiency of the technique (either beam-steering or beamforming) is compromised by two issues intrinsic to the TMA technique [21]:

1. The frequency behavior of conventional rectangular pulses, which are not the best ones to efficiently distribute the spectral energy among the multiple harmonic patterns to be exploited [20, 24].
2. The duplicated-specular radiation diagrams, which are a consequence of the presence of

*Declarations of interest: none.

**This work has been funded by the Xunta de Galicia (ED431C 2016-045, ED431G/01), the Agencia Estatal de Investigación of Spain (TEC2016-75067-C4-1-R) and ERDF funds of the EU (AEI/FEDER, UE).

*Corresponding author: José A. García-Naya, email: jagarcia@udc.es, phone: +34 881016086, postal address: Facultad de Informática, Campus de Elviña s/n, 15071 A Coruña, SPAIN.

Email addresses: roberto.maneiro@udc.es (Roberto Maneiro-Catoira), julio.bregains@udc.es (Julio Brégains), jagarcia@udc.es (José A. García-Naya), luis@udc.es (Luis Castedo)

[1]EURASIP member.

negative harmonics with the same magnitude and opposite phase. Additionally, the scanning inability of the fundamental mode beam and the proportionality between the phases of harmonics with different order apparently jeopardize the versatility of beamforming with TMAs [21]. A solution to the first issue is proposed in [11] by using single-pole double-throw (SPDT) switches —controlled by rectangular sequences with a duty cycle of 50%— and fixed 180° phase shifters. Such a structure generates only odd harmonics and removes the fundamental pattern, but does not solve the problem of the mirror-frequency diagrams.

A more efficient beam-steering architecture (with two single-pole single-throw (SPST) switches per antenna and some additional hardware such as one-bit phase shifters) is proposed in [34] to overcome the two aforementioned issues. Such a single-sideband (SSB) time-modulated phased array architecture synthesizes a steerable uniform beam in the first positive harmonic, and is capable of removing the third-order harmonics, being the highest undesired harmonic that of fifth order. However, the amplitude of such a uniform radiated pattern is still not reconfigurable.

Hence, if we want to reconfigure the amplitude pattern topology (e.g., in terms of side-lobe level (SLL)), while overcoming the aforementioned issues, non-switched TMA beamforming solutions provide excellent levels of power efficiency, but at the expense of increasing their complexity and, above all, with the handicap of the hardware implementation at high frequencies [21].

The motivation of this paper is the innovation in the design of switched TMAs towards the following directions:

1. The proposal of an SSB switched TMA scheme —based on the novel application of stair-step periodic pulses— to efficiently perform both beam-steering and beamforming, thus showing the ability of reconfiguring the radiated pattern amplitude.
2. The proposal of a hardware structure for such a switched TMA scheme, attractive in terms of cost, size, and complexity.
3. The application of the proposed structure to multibeam transceivers employing a single radio-frequency front-end and showing a performance conditioned by the signal bandwidth rather than the carrier frequency (as in the case of beamformers based on VPSs or non-switched TMAs).

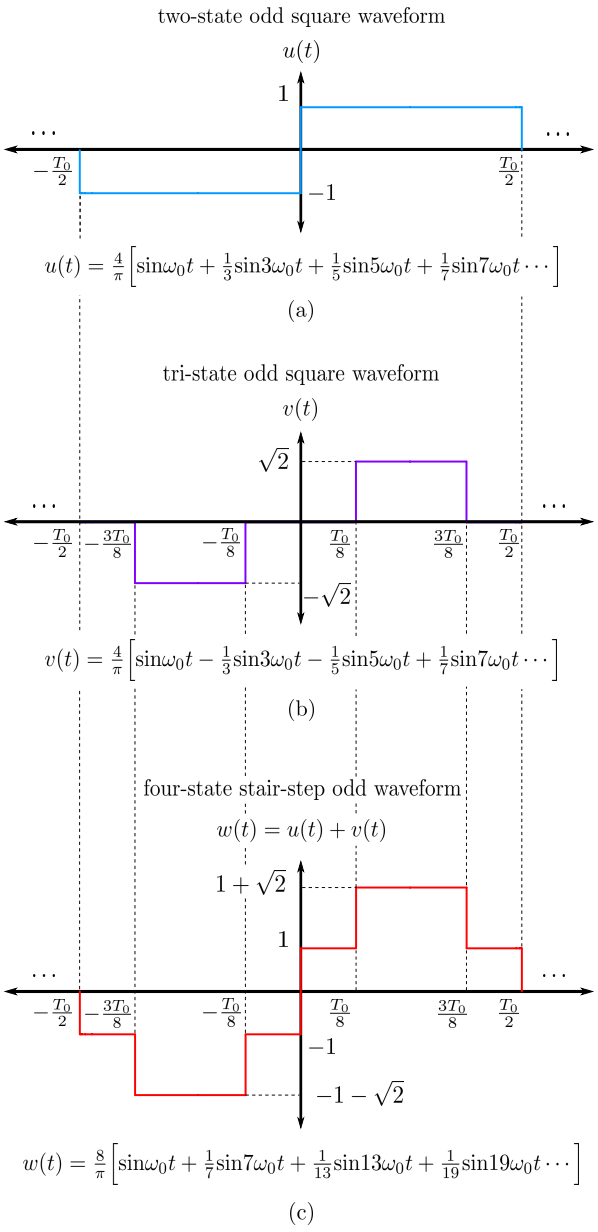

Figure 1: Periodic odd waveforms: (a) two-state square waveform with only odd harmonic components, (b) tri-state odd square periodic waveform which inverts the phase of the two harmonics in the middle out of every group of four harmonics, and (c) the sum of the previous waveforms that removes the aforementioned harmonics.

2. Characterization of Periodic Stair-Step Pulses

Since our objective is to efficiently exploit the first positive harmonic of a TMA, odd periodic rectangular pulses are particularly suitable (apart from its easy and cost-effective implementation) for the following reasons:

- Their direct current (DC) component is zero. Hence, the limitation of having radiation patterns with no steering capability, such as the fundamental one centered at the carrier frequency ω_c, is overcome [24].
- Their even harmonic components are also zero, thus providing an advantageous starting point in terms of efficiency with respect to other alternatives.

In the following, we look into more detail at these properties. Our point of departure is the simplest odd periodic pulse: the bipolar two-state square waveform $u(t)$ plotted in Fig. 1a. The Fourier coefficients of the periodic extension of such a signal, with fundamental period T_0, are given by

$$U_q = \frac{1}{T_0}\int_{-T_0/2}^{T_0/2} u(t)\mathrm{e}^{-jq\omega_0 t} = \begin{cases} 0 & q \text{ even} \\ -\frac{2j}{\pi q} & q \text{ odd,} \end{cases} \quad (1)$$

with $\omega_0 = 2\pi/T_0$. We observe that the spectral information is entirely contained in the odd harmonics. Notice also that $U_{-q} = U_q^*$, because $u(t) \in \mathbb{R}$. Since the modulus and the argument of U_q are $|U_q| = 2/(\pi q)$ and $\sphericalangle U_q = -\pi/2$, respectively, we can easily express the Fourier series expansion of $u(t)$ as (see Fig. 1a)

$$u(t) = \frac{4}{\pi}\sum_{q=1,3,5,\ldots}^{\infty} \frac{1}{q}\sin(q\omega_0 t). \quad (2)$$

Notice that when we apply this kind of pulses to a uniformly excited TMA [11, 10], we find that the peak level of the first undesired harmonic (the third one) is too high ($-9.54\,\mathrm{dB}$) with respect to the first-order harmonic peak, making these pulses very inefficient for our purposes. Hence, it would be desirable for our target pulses to eliminate the third and even the fifth order harmonics. To construct pulses with such features, we turned our attention to the tri-state odd square waveform $v(t)$ in Fig. 1b, whose Fourier series coefficients are

$$V_q = \frac{j\sqrt{2}}{q\pi}\left[\cos\left(\frac{3\pi q}{4}\right) - \cos\left(\frac{\pi q}{4}\right)\right] = \begin{cases} 0 & q \text{ even} \\ (-1)^{\frac{(q+1)(q-1)}{8}}\left(-\frac{2j}{\pi q}\right) & q \text{ odd,} \end{cases} \quad (3)$$

in which the sign of V_q is derived in Appendix A.1. Analogously to the pulse $u(t)$, the Fourier series expansion is easily derived from (3), arriving at (see also Fig. 1b)

$$v(t) = \frac{4}{\pi}\sum_{q=1,3,5,\ldots}^{\infty} (-1)^{\frac{(q+1)(q-1)}{8}}\frac{1}{q}\sin(q\omega_0 t). \quad (4)$$

As a result, the pulse $w(t) = u(t)+v(t)$ (see Fig. 1c) is a four-state stair-step odd waveform with Fourier series coefficients

$$W_q = U_q + V_q = \begin{cases} -\frac{4j}{\pi q} & |q| \in \Upsilon \\ 0 & \text{otherwise,} \end{cases} \quad (5)$$

with $\Upsilon = \{4\alpha + (-1)^\alpha - 2; \alpha \in \mathbb{N}^*\} = \{1, 7, 9, 15, 17, 23, 25, 31, \ldots\}$, and therefore

$$w(t) = \frac{8}{\pi}\sum_{q\in\Upsilon}\frac{1}{q}\sin(q\omega_0 t). \quad (6)$$

Additionally, and in order to steer the exploited TMA harmonic pattern, we must consider a time-shifted version of $w(t)$, $w_n(t) = w(t - D_n)$, with D_n being the corresponding time-delay variable, leading to

$$w_n(t) = \frac{8}{\pi}\sum_{q\in\Upsilon}\frac{1}{q}\sin(q\omega_0(t - D_n)). \quad (7)$$

In the following sections, we consider the pulse $w_n(t)$ to efficiently design a flexible SSB TMA beamformer.

3. SSB TMA Beamformer Using Periodic Stair-Step Pulses

Let us consider a linear array with N isotropic elements with unitary static excitations $I_n = 1$, $n \in \{0, 1, \ldots, N-1\}$, whose n-th element feeding scheme is illustrated in Fig. 2. The phase and the amplitude of the n-th dynamic excitation of the array are controlled separately. More specifically, the phase is controlled with a two-branch structure: one branch is time-modulated by a stair-step periodic

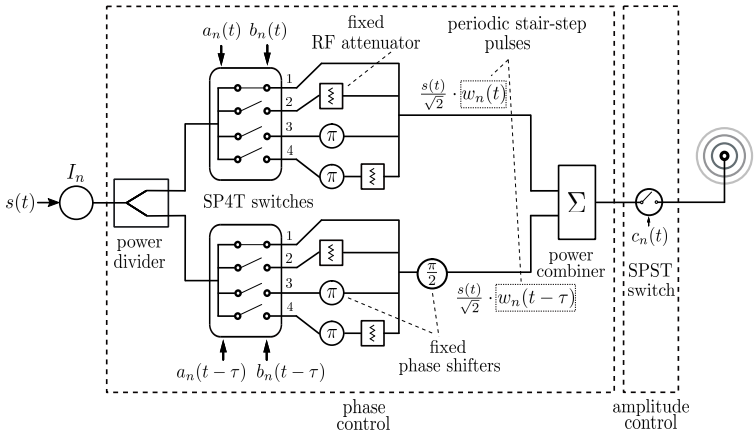

Figure 2: Feeding scheme for the n-th antenna element of the proposed SSB TMA beamformer, being $w_n(t)$ a periodic stair-step pulse, $c_n(t)$ a periodic rectangular pulse, and τ a time-delay. The phase and the amplitude of the corresponding time-modulated excitation are controlled separately.

(T_0) waveform $w_n(t)$, whereas the other one is time-modulated by $w_n(t-\tau)$, with τ being a previously fixed time delay, followed by a $\pi/2$ fixed phase shifting. On the other hand, the amplitude is controlled by a periodic (T_0) rectangular pulse $c_n(t)$ generated by means of an SPST switch.

Let us see in detail how $w_n(t)$ and $w_n(t-\tau)$ are applied to the n-th array excitation (Fig. 2). The four levels of the stair-step pulse are generated by means of a single-pole four-throw (SP4T) switch controlled by the periodic (T_0) binary signals $a_n(t)$ and $b_n(t)$ whose states are specified in Table 1.

More specifically, the switch terminals are connected physically to the antenna according to:

- Terminal 1: direct connection.
- Terminal 2: connection through a fixed radio frequency (RF) attenuator of $-20\log(1+\sqrt{2})$ dB.
- Terminal 3: connection through a fixed 180° phase shifter.
- Terminal 4: connection through a fixed phase shifter followed by a fixed RF attenuator, both with the same characteristics as those employed in Terminal 3 and Terminal 2 branches, respectively.

The second SP4T switch is used to apply the delayed periodic pulse $w_n(t-\tau)$ to the n-th array excitation. Such a switch is controlled by the corresponding delayed versions of $a_n(t)$ and $b_n(t)$.

According to Fig. 2, the time-varying array factor will be given by

$$F(\theta,t)=\sum_{n=0}^{N-1} c_n(t)\left[\frac{w_n(t)}{\sqrt{2}}+j\frac{w_n(t-\tau)}{\sqrt{2}}\right]\mathrm{e}^{j\beta z_n\cos\theta}, \tag{8}$$

where z_n represents the n-th array element position on the z axis, θ is the angle with respect to such a main axis, $\beta=2\pi/\lambda$ represents the wavenumber for a carrier wavelength $\lambda=2\pi\mathrm{c}/\omega_c$, where c is the speed of light and ω_c is the carrier frequency of the communication signal $s(t)$ shown in Fig. 2. Notice that ω_c is not explicitly included in the array factor in (8) as in previous works [22, 25]. We begin the analysis of (8) by evaluating the term $w_n(t)+jw_n(t-\tau)$. For the sake of simplicity, we will analyze the Fourier transform (FT) of such a term, i.e., $\mathrm{FT}[w_n(t)]+j\mathrm{FT}[w_n(t-\tau)]$ where, by virtue of (7),

$$\begin{aligned}&\mathrm{FT}[w_n(t)]=\\&=\frac{8}{j}\sum_{q\in\Upsilon}\frac{1}{q}[\mathrm{e}^{-jq\omega_0 D_n}\delta(\omega-q\omega_0)-\mathrm{e}^{jq\omega_0 D_n}\delta(\omega+q\omega_0)],\end{aligned}$$

and

$$\begin{aligned}&\mathrm{FT}[w_n(t-\tau)]=\mathrm{e}^{-j\omega\tau}\mathrm{FT}[w_n(t)]=\\&=\frac{8}{j}\sum_{q\in\Upsilon}\frac{1}{q}[\mathrm{e}^{-jq\omega_0\tau}\mathrm{e}^{-jq\omega_0 D_n}\delta(\omega-q\omega_0)-\\&-\mathrm{e}^{jq\omega_0\tau}\mathrm{e}^{jq\omega_0 D_n}\delta(\omega+q\omega_0)],\end{aligned} \tag{9}$$

where $\delta(\omega)$ is the unit impulse in the frequency domain. If we select a delay τ verifying that $\omega_0\tau=$

$\pi/2$, then $\mathrm{e}^{-jq\omega_0\tau} = (-j)^q$ and $\mathrm{e}^{jq\omega_0\tau} = j^q$, and hence we have that

$$\begin{aligned}&\mathrm{FT}[w_n(t)] + j\mathrm{FT}[w_n(t-\tau)] = \\ &= \frac{8}{j}\sum_{q\in\Upsilon}\frac{1}{q}\Bigg[(1-(-j)^{q+1})\mathrm{e}^{-jq\omega_0 D_n}\delta(\omega - q\omega_0) + \\ &+ (-1-j^{q+1})\mathrm{e}^{jq\omega_0 D_n}\delta(\omega + q\omega_0)\Bigg]. \end{aligned} \tag{10}$$

Considering the sets of indexes $\Upsilon_1 = \{8\alpha - 7; \alpha \in \mathbb{N}^*\} = \{1, 9, 17, \dots\}$ and $\Upsilon_2 = \{8\alpha - 1; \alpha \in \mathbb{N}^*\} = \{7, 15, 23, \dots\}$, verifying $\Upsilon = \Upsilon_1 \cup \Upsilon_2$, we realize that

$$\begin{aligned}1-(-j)^{q+1} &= \begin{cases}2 & q\in\Upsilon_1 \\ 0 & q\in\Upsilon_2,\end{cases}; \\ -1-j^{q+1} &= \begin{cases}-2 & q\in\Upsilon_2 \\ 0 & q\in\Upsilon_1.\end{cases}\end{aligned} \tag{11}$$

Hence, we rewrite (10) as

$$\begin{aligned}&\mathrm{FT}[w_n(t)] + j\mathrm{FT}[w_n(t-\tau)] = \\ &= \frac{16}{j}\sum_{q\in\Upsilon_1}\frac{1}{q}\mathrm{e}^{-jq\omega_0 D_n}\delta(\omega - q\omega_0) + \\ &+ \frac{(-16)}{j}\sum_{q\in\Upsilon_2}\frac{1}{q}\mathrm{e}^{jq\omega_0 D_n}\delta(\omega + q\omega_0),\end{aligned} \tag{12}$$

and we realize that the harmonics with order $-1, 7, -13, 19, \dots$ are removed. By applying the inverse FT to (12), we have

$$\begin{aligned}&w_n(t) + jw_n(t-\tau) = \\ &= \sum_{q\in\Upsilon_1}\frac{8}{j\pi q}\mathrm{e}^{-jq\omega_0 D_n}\mathrm{e}^{jq\omega_0 t} \\ &+ \sum_{q\in\Upsilon_2}\frac{(-8)}{j\pi q}\mathrm{e}^{jq\omega_0 D_n}\mathrm{e}^{-q\omega_0 t}.\end{aligned} \tag{13}$$

Table 1: Control of an SP4T switch (during one period T_0) to time-modulate the array excitations with the stair-step periodic signal $w_n(t)$ in Fig. 1c. The position of the SP4T switch is determined by the corresponding levels of the switch control periodic (T_0) signals $a_n(t)$ and $b_n(t)$.

$a_n(t)$	$b_n(t)$	SP4T output	$w_n(t)$
0	0	1	$1+\sqrt{2}$
0	1	2	1
1	0	3	$-1-\sqrt{2}$
1	1	4	-1

On the other hand, the Fourier series expansion of $c_n(t)$ is given by

$$c_n(t) = \sum_{k=-\infty}^{\infty} C_{nk}\mathrm{e}^{jk\omega_0 t}, \tag{14}$$

with $C_{nk} = \xi_n \mathrm{sinc}(k\pi\xi_n)\mathrm{e}^{-jk\pi\xi_n}$ [13]. In this expression, $\mathrm{sinc}(x) = \sin(x)/x$, and $\xi_n \in (0, 1] \subset \mathbb{R}$ are the normalized pulse time durations. By considering (13) and (14), we can rewrite (8) as

$$\begin{aligned}&F(\theta,t) = \\ &= \frac{1}{\sqrt{2}}\sum_{n=0}^{N-1}\Bigg[\sum_{k=-\infty}^{\infty}C_{nk}\mathrm{e}^{jk\omega_0 t}\Bigg(\sum_{q\in\Upsilon_1}\frac{8}{j\pi q}\mathrm{e}^{-jq\omega_0 D_n}\mathrm{e}^{jq\omega_0 t} \\ &+ \sum_{q\in\Upsilon_2}\frac{(-8)}{j\pi q}\mathrm{e}^{jq\omega_0 D_n}\mathrm{e}^{-jq\omega_0 t}\Bigg)\Bigg] \\ &= \frac{1}{\sqrt{2}}\sum_{k=-\infty}^{\infty}\sum_{q\in\Upsilon_1}\mathrm{e}^{j(k+q)\omega_0 t} \\ &\cdot \sum_{n=0}^{N-1}\underbrace{C_{nk}\tfrac{8}{j\pi q}\mathrm{e}^{-jq\omega_0 D_n}}_{=(I_n)_q^k}\mathrm{e}^{jkz_n\cos\theta} \\ &+ \frac{1}{\sqrt{2}}\sum_{k=-\infty}^{\infty}\sum_{q\in\Upsilon_2}\mathrm{e}^{j(k-q)\omega_0 t} \\ &\cdot \sum_{n=0}^{N-1}\underbrace{C_{nk}\tfrac{(-8)}{j\pi q}\mathrm{e}^{jq\omega_0 D_n}}_{=(I_n')_q^k}\mathrm{e}^{jkz_n\cos\theta}.\end{aligned} \tag{15}$$

We now define

$$\begin{aligned}F_1(\theta,t)_q^k &= \mathrm{e}^{j(k+q)\omega_0 t}\sum_{n=0}^{N-1}(I_n)_q^k\cdot\mathrm{e}^{jkz_n\cos\theta}, \\ F_2(\theta,t)_q^k &= \mathrm{e}^{j(k-q)\omega_0 t}\sum_{n=0}^{N-1}(I_n')_q^k\cdot\mathrm{e}^{jkz_n\cos\theta},\end{aligned} \tag{16}$$

where the dynamic excitations $(I_n)_q^k$ and $(I_n')_q^k$ are given by

$$\begin{aligned}(I_n)_q^k &= \frac{8C_{nk}}{j\pi\sqrt{2}q}\mathrm{e}^{-jq\omega_0 D_n},\ \ q\in\Upsilon_1,\ \ k\in\mathbb{Z}, \\ (I_n')_q^k &= \frac{-8C_{nk}}{j\pi\sqrt{2}q}\mathrm{e}^{jq\omega_0 D_n},\ \ q\in\Upsilon_2,\ \ k\in\mathbb{Z},\end{aligned} \tag{17}$$

to finally obtain

$$F(\theta,t) = \sum_{k=-\infty}^{\infty}\left[\sum_{q\in\Upsilon_1}F_1(\theta,t)_q^k + \sum_{q\in\Upsilon_2}F_2(\theta,t)_q^k\right]. \tag{18}$$

Notice that we must consider the normalized version of the pulses in Fig. 1c since we are not considering a voltage gain of $1+\sqrt{2}$ at the input of the SP4Ts. Consequently, the normalized dynamic excitations are

$$(\overline{I_n})_q^k = \frac{8C_{nk}}{j\sqrt{2}(1+\sqrt{2})\pi q} \mathrm{e}^{-jq\omega_0 D_n}, \quad q \in \Upsilon_1, \quad k \in \mathbb{Z},$$
$$(\overline{I_n'})_q^k = \frac{-8C_{nk}}{j\sqrt{2}(1+\sqrt{2})\pi q} \mathrm{e}^{jq\omega_0 D_n}, \quad q \in \Upsilon_2, \quad k \in \mathbb{Z}, \tag{19}$$

and therefore, $|(\overline{I_n})_q^k|^2 = |(\overline{I_n'})_q^k|^2 = 32|C_{nk}|^2/((1+\sqrt{2})\pi q)^2$. Notice that C_{nk} will be selected in the conventional way of TMA design, i.e., using systematic optimization algorithms to maintain the side-lobe zone of the radiated power of the fundamental mode $k=0$ under a certain and previously stipulated level, whereas the radiated power over the undesired harmonics is minimized. Hence, only $C_{n0} = \xi_n$ will be meaningful in the SSB TMA pattern design. Once $k=0$ is considered, the two most significant $|(\overline{I_n})_q^k|^2$ are those for $q = 1 \in \Upsilon_1$ and for $q = 7 \in \Upsilon_2$, hence satisfying that $20\log|(\overline{I_n})_7^0/(\overline{I_n})_1^0| = -16.9$ dB. Therefore, the aim of the technique is to guarantee a single useful harmonic beam pattern: the one given by $|F_1(\theta,t)_1^0|^2$.

4. Efficiency of the Time Modulation

In this section we determine the efficiency of the time modulation operation in the proposed SSB TMA beamformer. For the sake of simplicity, but without any relevant loss of generality, we will consider a uniform linear array with $\lambda/2$ of inter-element distance transmitting a single carrier with normalized power. Such an efficiency can be split into two separate efficiencies

$$\eta = \eta_{\mathrm{TMA}} \cdot \eta_{\mathrm{BFN}}, \tag{20}$$

whose interpretations are described below. The term η_{TMA} accounts for the ability of the TMA technique to radiate only over the useful harmonics. It is determined by

$$\eta_{\mathrm{TMA}} = \frac{P_U^{\mathrm{TM}}}{P_R^{\mathrm{TM}}}, \tag{21}$$

where P_U^{TM} and P_R^{TM} are the useful and the total mean powers, respectively, radiated by the SSB TMA beamformer. It is remarkable that the SSB operation at least doubles the value of this efficiency with respect to that of a conventional TMA.

Most of the works available in the literature analyzing the TMA efficiency limit themselves to the study of η_{TMA}. The second component of the efficiency, η_{BFN}, accounts for the reduction of the total mean power radiated by a uniform static array caused by the insertion of the TMA BFN. η_{BFN} is of critical importance due to its high impact on the antenna gain. This efficiency is evaluated by means of the quotient

$$\eta_{\mathrm{BFN}} = \frac{P_R^{\mathrm{TM}}}{P_R^{\mathrm{ST}}}, \tag{22}$$

where P_R^{ST} is the total mean power radiated by a uniform static array with N elements.

Let us now analyze in detail both efficiencies. We will start by deriving the expression of η_{TMA}. In the proposed design, P_R^{TM} is given by [24]

$$P_R^{\mathrm{TM}} = \sum_{k=-\infty}^{\infty} \left[\sum_{q\in\Upsilon_1} (p_1)_q^k + \sum_{q\in\Upsilon_2} (p_2)_q^k \right], \tag{23}$$

being $(p_1)_q^k$ and $(p_2)_q^k$ the mean transmit power values at the harmonics $\omega_c + (k+q)\omega_0$ and $\omega_c + (k-q)\omega_0$, respectively. Since $(p_1)_q^k = (p_2)_q^k = 4\pi\sum_{n=0}^{N-1}|(\overline{I_n})_q^k|^2$ [24], by considering (19), we have

$$(p_1)_q^k = (p_2)_q^k = \frac{128}{\pi(1+\sqrt{2})^2} \sum_{n=0}^{N-1} \xi_n^2 \,\mathrm{sinc}^2(k\pi\xi_n)/q^2. \tag{24}$$

Thus, we can rewrite (23) as

$$P_R^{\mathrm{TM}} = \frac{128}{\pi(1+\sqrt{2})^2} \sum_{n=0}^{N-1} \sum_{q\in\Upsilon} \sum_{k=-\infty}^{\infty} \frac{\xi_n^2 \,\mathrm{sinc}^2(k\pi\xi_n)}{q^2}. \tag{25}$$

Having now in mind that for all $\xi_n \in (0,1]$ the sinc-square infinite series converges to $\sum_{k=-\infty}^{\infty}\mathrm{sinc}^2(k\pi\xi_n) = 1/\xi_n$, we can express the total mean power as

$$P_R^{\mathrm{TM}} = \frac{128}{\pi(1+\sqrt{2})^2} \sum_{q\in\Upsilon} \frac{1}{q^2} \sum_{n=0}^{N-1} \xi_n, \tag{26}$$

and since the infinite series $\sum_{q\in\Upsilon} 1/q^2 = 1/64\,(\Psi_1(1/8) + \Psi_1(7/8))$, with Ψ_1 the polygamma function of order 1 (see Appendix A.2), by denoting $A_0 = \sum_{q\in\Upsilon} 1/q^2 = 1.053$, we then arrive at the

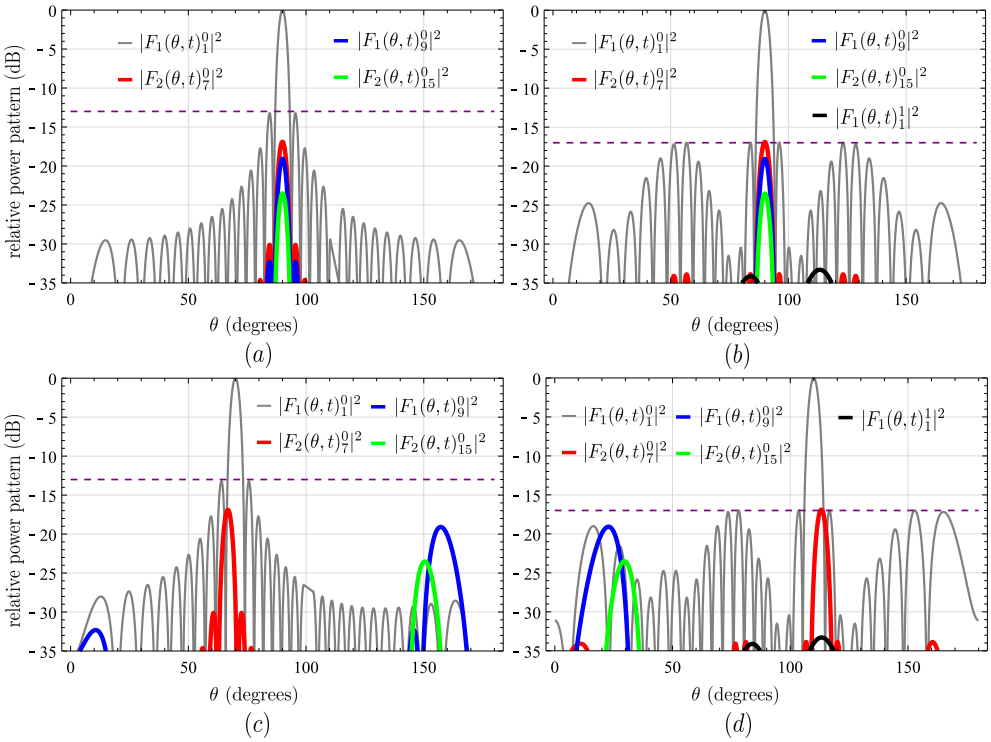

Figure 3: By considering an array of $N = 30$ elements treated as the one illustrated in Fig. 2, we show the normalized power radiated patterns for the following TMA configurations: (a) Phased array mode (SPST switches closed) with $D_n = 0$ ($\theta_{\text{scan}} = 90°$). The first undesired harmonic, at $\omega_c - 7\omega_0$, has a -16.90 dB peak level. The subsequent harmonics, at $\omega_c + 9\omega_0$ and $\omega_c - 15\omega_0$, have peak levels of -19.08 dB and -23.52 dB, respectively. The efficiency of the time modulation is $\eta = 0.56$ (-2.55 dB). (b) Beamformer mode with $D_n = 0$ ($\theta_{\text{scan}} = 90°$). The SPST switches are governed by periodic sequences with the ξ_n values specified in Table 2. The SLL of the desired pattern is now set at -17 dB. Notice that, apart from the undesired harmonics of the phased array mode, the most significant harmonic due to the amplitude time modulation is the one corresponding to $\omega_c + 2\omega_0$, which is below -30 dB. The price to be paid for the SLL improvement is a certain worsening of the efficiency: $\eta = 0.46$ (-3.37 dB). (c) Phased array mode with D_n selected to accomplish a $\theta_{\text{scan}} = 70°$. (d) Beamformer mode with D_n selected to accomplish a $\theta_{\text{scan}} = 110°$.

ensuing compact expression

$$P_R^{\text{TM}} = \frac{128A_0}{\pi(1+\sqrt{2})^2}\sum_{n=0}^{N-1}\xi_n. \tag{27}$$

On the other hand, the useful mean radiated power is $P_U^{\text{TM}} = (p_1)_1^0$ and, by virtue of (24), we have that

$$P_U^{\text{TM}} = \frac{128}{\pi(1+\sqrt{2})^2}\sum_{n=0}^{N-1}\xi_n^2, \tag{28}$$

and by substituting (27) and (28) into (21), we have

$$\eta_{\text{TMA}} = \frac{\sum_{n=0}^{N-1}\xi_n^2}{A_0\sum_{n=0}^{N-1}\xi_n}. \tag{29}$$

Regarding the term η_{BFN}, by quantifying P_R^{ST} as the total mean transmitted power over the array factor $F^{\text{ST}}(\theta) = \sum_{n=0}^{N-1} \text{e}^{jkz_n\cos\theta}$, we have

$$P_{\text{R}}^{\text{ST}} = \int_0^{2\pi}\int_0^{\pi}|F^{\text{ST}}(\theta)|^2\sin(\theta)\text{d}\theta\text{d}\varphi = 4\pi N. \tag{30}$$

By substituting (27) and (30) into (22), we arrive at

$$\eta_{\text{BFN}} = \frac{32A_0\sum_{n=0}^{N-1}\xi_n}{\pi^2(1+\sqrt{2})^2 N}. \tag{31}$$

5. Numerical Examples

In this section we examine the behavior of the proposed TMA in its two possible configurations: (1) basic (or phased array) mode, with only phase weighting of the array excitations; and (2) full-featured (or beamformer) mode, with amplitude-phase weighting of the array excitations.

5.1. Phased Array Mode

Let us consider a uniform linear array with $N = 30$ elements spaced $d = \lambda/2$ apart with unitary static excitations treated as the one illustrated in Fig. 2. We configure the TMA by setting $c_n(t) = 1$ and, hence, the SPST switches are permanently closed. In other words, k is set to zero and $C_{n0} = 1,\ n \in \{0, 1, \ldots, N-1\}$. Initially, the time-delays D_n are also set to zero, hence the scanning angle of all patterns (see (19)) will be $\theta_{\text{scan}} = 90°$. Fig. 3a illustrates that the proposed scheme is capable of concentrating the radiated power on the desired first harmonic pattern, $|F_1(\theta,t)_1^0|^2$, located at $\omega_c + \omega_0$. The most meaningful unwanted harmonic patterns —in decreasing order of significance— are: $|F_2(\theta,t)_7^0|^2$ at $\omega_c - 7\omega_0$, $|F_1(\theta,t)_9^0|^2$ at $\omega_c + 9\omega_0$, and $|F_2(\theta,t)_{15}^0|^2$ at $\omega_c - 15\omega_0$. It is remarkable that the highest peak level of the unwanted harmonics (-16.90 dB, corresponding to $\omega_c - 7\omega_0$) is approximately 4 dB below the level of the main secondary lobes (-13 dB) of the desired pattern at $\omega_c + \omega_0$. The subsequent harmonics, at $\omega_c + 9\omega_0$ and $\omega_c - 15\omega_0$, have peak levels of -19.08 dB and -23.52 dB, respectively. On the other hand, by virtue of (20), (29) and (31), the corresponding efficiencies[2] are $\eta_{\text{TMA}} = 0.96$ (-0.16 dB) and $\eta_{\text{BFN}} = 0.58$ (-2.39 dB), leading to $\eta = 0.56$ (-2.55 dB).

Fig. 3c illustrates the scanning capability of the proposed TMA scheme. The D_n values are selected to accomplish a $\theta_{\text{scan}} = 70°$ by simply assigning progressive phases to the array elements. Notice that the D_n values (see (24)) have no effect on the efficiency. Also, as we are exclusively performing a phase weighting of the array excitations, the radiated power patterns in Figs. 3a and 3c are, necessarily, uniform.

5.2. Beamformer Mode

In this mode, the SPST switches are governed by the periodic sequences $c_n(t)$. Fig. 3b illustrates the normalized power radiated pattern when D_n are set to zero ($\theta_{\text{scan}} = 90°$) and the normalized pulse durations ξ_n of the modulating sequences $c_n(t)$ are those in Table 2. Such time durations were obtained by means of a simulating annealing algorithm as explained in [13]. Under the assumption of symmetric dynamic excitations, for each index q, the optimization algorithm is capable (in this example) of setting the SLL of the desired pattern ($k = 0$) to -17 dB, while the remainder harmonics patterns ($k \neq 0$) are kept below -30 dB. Notice that, due to this additional time modulation, apart from the undesired harmonics of the phased array mode (associated to different indexes q and whose corresponding SLL are also set to -17 dB with respect to their maxima), other harmonic patterns are generated, as it was analyzed in Section 3. Among them, the most significant is $|F_1(\theta,t)_1^1|^2$ at $\omega_c + 2\omega_0$ which, as we can observe, is below -30 dB. The price to be paid for the SLL improvement is a certain worsening of the TMA efficiencies: $\eta_{\text{TMA}} = 0.91$ (-0.41 dB) and $\eta_{\text{BFN}} = 0.50$ (-3.01 dB), leading to $\eta = 0.46$ (-3.42 dB). Fig. 3d illustrates both the scanning and the amplitude reconfiguration capabilities of the proposed TMA by showing the normalized power radiated pattern when D_n are selected to accomplish a $\theta_{\text{scan}} = 110°$, whereas $c_n(t)$ are the same as those in Fig. 3b.

The results in Figs. 3b and 3d are similar to those presented in [34]. Nevertheless, the architecture proposed in this work allows for a maximum signal bandwidth $B_{\max} = 8f_0$ (the first unwanted harmonic is $q = -7$), whereas in [34], $B_{\max} = 4f_0$, and hence, improving the bandwidth response of the TMA by 100%.

Notice that the proposed architecture handles two types of time parameters:

1. The time delays D_n for the modulating signals, which are selected to synthesize progressive phases, i.e., $D_n/T_0 = n\cos(\theta_{\text{scan}})$, where θ_{scan} is the direction of the first positive harmonic beam.
2. The pulse durations, ξ_n, corresponding to the on-state duration of the rectangular pulses that govern $c_n(t)$. The values of ξ_n are obtained by means of an optimization algorithm [12]

Table 2: Normalized pulse durations of the sequences that govern the SPST switches shown in Fig. 2. ξ_n values are provided in [13] where symmetric dynamic excitations are considered in an array of $N = 30$ elements. Hence, $n \in \{0, 1, \ldots, 29\}$.

element	1, 28	2, 27	3, 26	4, 25	5, 24	9, 20	others
ξ_n	0.136	0.050	0.953	0.947	0.689	0.926	1

[2] Throughout this paper we express the efficiencies both in natural units (as defined in (29), (31) and (20)) and in dB, i.e., as $10\log_{10}(\cdot)$ of the corresponding efficiencies. The latter is more convenient to specify the power losses of the TMA.

which selects the Fourier coefficients of $c_n(t)$, $C_{nk} = \xi_n \operatorname{sinc}(k\pi\xi_n)\mathrm{e}^{-jk\pi\xi_n}$, to obtain a radiation diagram for $k = 0$ with a given SLL, whereas the rest of harmonics ($k \neq 0$) are kept below a threshold.

With respect to the scanning ability of the TMA, we observe in Fig. 4 a TMA scanning range of ± 68 degrees from the broad sight direction. Although the threshold level of the unwanted harmonics is not being affected by the steering of the beam, the half power beam width of the exploited harmonic widens as it moves away from the center.

On the other hand, we have analyzed the impact of the rise-fall times of the switches (see Fig. 5), and we have realized that there is a time interval (and hence we can select an adequate switch, as in [26, 34]), during which the switches can be profitably used to decrease the peak level of the unexploited harmonics, thus improving η_{TMA}. However, this is achieved at the expense of reducing the overall time modulation efficiency, η, and degrading the TMA frequency performance because, due to the appearance of new harmonics, the time modulation frequency must be duplicated to faithfully send (receive) signals with the same bandwidth as in the case of considering ideal pulses.

We have considered a rise-fall time $0.06T_0$ together with a set of ξ_n (see Table 3) to ensure that SLL $= -20\,\mathrm{dB}$ and a threshold for the harmonics equal to $-20\,\mathrm{dB}$. Fig. 6 shows the corresponding power radiated pattern. With respect to the TMA efficiencies we obtain: $\eta_{\mathrm{TMA}} = 0.99$ ($\eta_{\mathrm{TMA}} = -0.04\,\mathrm{dB}$) and $\eta_{\mathrm{BFN}} = 0.36$ ($\eta_{\mathrm{BFN}} = -4.45\,\mathrm{dB}$), leading to $\eta = 0.35$ ($\eta = -4.49\,\mathrm{dB}$). We observe a trade-off between the SLL and the overall efficiency of the TMA and that, in any case, the total insertion losses introduced by the TMA technique are lower than those corresponding to off-the-shelf VPSs (see Fig. 9).

Table 3: Normalized nonideal pulse durations of the sequences that govern the SPST switches shown in Fig. 2.

element	2	4	5	6	7
ξ_n	0.063	0.078	0.076	0.063	0.880
element	14	18	19	20	
ξ_n	0.962	0.175	0.471	0.977	

6. Features of the SSB TMA Beamformer

In this section we discuss some practial issues regarding the proposed SSB TMA beamforming technique. In particular, we show the advantages of the proposed scheme with respect to conventional beam scanning antenna systems in relation to the following aspects:

1. **Cost**: a common feature to all high frequency reconfigurable devices is the significant increased cost with respect to their non-reconfigurable or fixed counterparts. For example, tunable phase shifters (e.g., [2, 3, 4, 6, 7]) are still an expensive option when compared to fixed broadband phase shifters, which can be manufactured using low-cost printed circuit board technology [8]. A similar reasoning can be applied to fixed RF attenuators [5] with respect to variable ones [7]. On the other hand, the use of SP4T switches provides a cost-effective solution (see e.g., [2]) to carry out the time modulation with stair-step periodic pulses. We could consider other non-switched alternatives, e.g., by using variable gain amplifiers (VGAs) [21, 23] or analog multipliers [23].
   Nevertheless, the implementation of the time modulation requires such devices be suitable to work in the band of the carrier frequency. As a matter of fact, these devices perform the time modulation by properly processing the transmitted signal at the antenna level, either modulating such a signal in amplitude or multiplying it by a periodic pulse. Therefore, an increase in the carrier frequency translates to a significant cost increase. For instance, if the TMA beam scanning operates at a carrier frequency ω_c, it is enough that the SP4T switches be suitable to work at the signal bandwidth B regardless of ω_c, whereas the VGAs or the analog multipliers must work at ω_c.
2. **Complexity**: when we are restricted to a single-beam exploitation, non-switched TMA architectures [21, 23] are apparently more complex not only in terms of hardware (especially if the devices have analog control due to the requirements of the digital-to-analog converters (DACs)), but also in terms of software. Whereas SP4T switches are governed by the switch-on and switch-off time instants of binary sequences, non-switched TMAs are capable of constructing, in the digital domain,

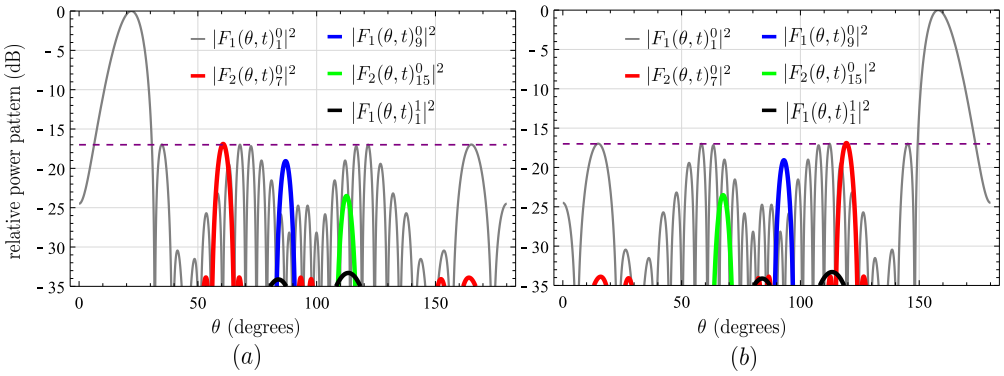

Figure 4: Normalized power radiated pattern showing a TMA scanning range of ±68° from the broad sight direction. The TMA is configured in the beamforming mode with the pulse durations ξ_n in Table 2. The threshold level of the unwanted harmonics is not being affected by the beam steering, but the half power beam width of the exploited harmonic widens as it moves away from the center.

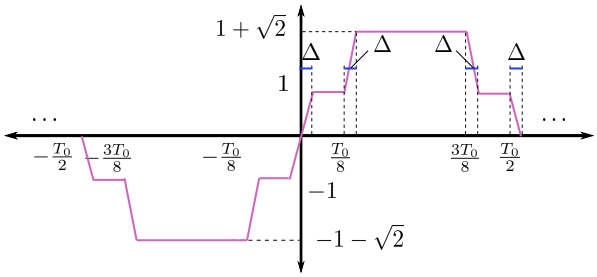

Figure 5: Nonideal stair step pulse. We have considered a rise-fall time of the SP4T switches, Δ, and a linear response of the transient, analogously to [34, 26].

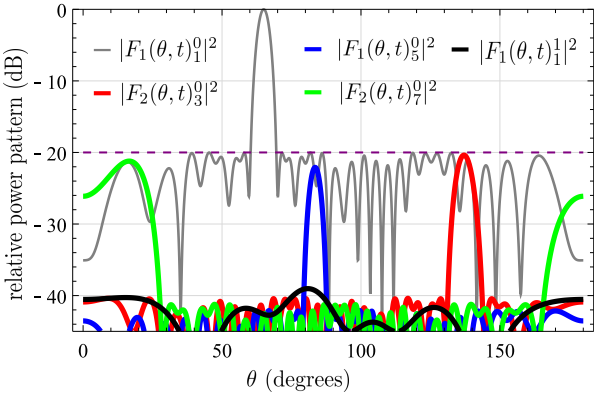

Figure 6: Normalized power radiated pattern of a TMA employing nonideal stair step pulses with a rise-fall time equal to $0.06T_0$ and considering the set of ξ_n specified in Table 3 to ensure that SLL = −20 dB. The threshold for the harmonics is equals to −20 dB, hence improving the efficiency, η_{TMA}, but at the expense of degrading the overall efficiency, verifying the trade-off between the SLL and the overall efficiency. As a matter of fact, we have obtained: $\eta_{\text{TMA}} = 99.0\%$ and $\eta_{\text{BFN}} = 35.8\%$, leading to $\eta = 35.5\%$ ($\eta = -4.45$ dB).

other complex waveforms, such as the sum-of-weighted-cosines (SWC) pulses [23] or pre-processed rectangular pulses [21]. Although non-switched TMAs can perform multibeam harmonic beamforming, they have the serious handicap of their hardware implementation at high frequencies (VGAs fast enough to follow a wideband signal, e.g., with a bandwidth of 1 GHz, or analog multipliers at the millimeter wave band).

On the other hand, it is well-known that TMA is a bandwidth-limited technique because, in general, the time modulation frequency (f_0) must satisfy that $B < f_0$, with B being the signal bandwidth. Such a restriction is necessary to avoid spectral overlapping between the signal replicas located at adjacent harmonics [19]. In our proposal, as the harmonics up to the seventh order are removed, the restriction becomes $B < 8f_0$, and hence it is possible to handle signal bandwidths eight times bigger than those handled by multibeam TMAs. As we have seen in Sections 1 and 2, the mathematical background of the TMAs synthesized in this work consists in approximating a pure sinusoid (a single harmonic) by means of stair-step pulses, while keeping the remaining (and inherently generated) harmonics below a threshold. Therefore, the ability of efficiently synthesizing a sum of pure sinusoids with SPMT switches for beamforming purposes paves the road for future investigations. Nevertheless, a promising applica-

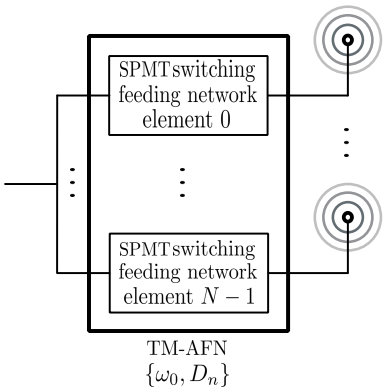

Figure 7: Block diagram of the overall TM-AFN in terms of the individual SPMT feeding networks of each element (see Fig. 2), specifying the fundamental frequency of the periodic pulses ω_0, and their time delays D_n.

tion of the proposed TMA feeding network is the transmission (reception) of multiple signals through the same antenna array with different spatial signatures.

Fig. 7 shows the block diagram of the overall TM-AFN corresponding to the proposed architecture. Notice that such a TM-AFN is characterized by the time-modulation frequency ω_0 and the time-delays D_n of the periodic pulses. Let us consider a transceiver capable of transmitting M linearly modulated digital signals over the downlink frequency ω_{DL} using different spatial signatures as well as capable of receiving M signals with different direction of arrivals (DoAs) over the uplink frequency ω_{UL}. To this end, we consider the multibeam transceiver architecture shown in Fig. 8, which is equipped with M TM-AFNs such as the one shown in Fig. 7.

In the downlink, each complex-valued baseband signal s_i, $i \in \{1, \cdots, M\}$, is I/Q modulated at a different intermediate frequency, $\omega_I - i\omega_0$. The I/Q modulated digital signal is then converted to the analog domain by using a single DAC with a sampling frequency higher than twice the total bandwidth of the composite signal. The obtained analog signal is up-converted to the downlink frequency, ω_{DL}. Next, each individual signal located at $\omega_{\mathrm{DL}} - i\omega_0$ is filtered out by the corresponding duplexer (equipped with a passband filter centered at such a frequency) before being processed by the corresponding i-th TM-AFN, which will shift the incoming signal in frequency to the downlink frequency ω_{DL} and will endow it with a spatial signature controlled by D_n, while keeping the undesired harmonics below a threshold level.

With respect to the uplink, the different harmonic patterns are designed to hold spatial orthogonality and, hence, at the output of the i-th TM-AFN, we have the corresponding received signal r_i located at $\omega_{\mathrm{UL}} + i\omega_0$. After crossing the corresponding duplexers, all the received signals at $\omega_{\mathrm{UL}} + i\omega_0$, $i \in \{1, \ldots, M\}$, are combined and down-converted to the intermediate frequency, ω_I. The obtained signal is next sampled at a frequency higher than twice the total signal bandwidth in order to be converted to the digital domain by a single ADC. Each digital signal is I/Q decomposed at a different intermediate frequency $\omega_I + i\omega_0$ to obtain the baseband complex signal r_i. We highlight that, in contrast to antenna arrays with VPS architectures [15, Fig. 10], TMAs employ a single down- (up-) converter and a single ADC (DAC), although requiring a wider bandwidth.

In sum, when compared to multibeam non-switched TMAs, the proposed multibeam structure is feasible at high frequencies although requiring a higher complexity. Nevertheless, it is also true that our proposal is less complex than the non-switched alternatives when we are restricted to the exploitation of a single beam. When compared to multibeam arrays based on VPSs and amplifiers, the proposed TMA solution only needs a single down- (up-) converter and a single ADC (DAC).

3. **Size**: when mobility at high frequencies is indispensable, the size is a crucial aspect. In this sense, RF switches and fixed attenuators are available as monolithic microwave integrated circuit (MMIC) devices [5, 2], while fixed phase shifters can be manufactured, for instance, using printed circuit board technology [8].
4. **Performance**: a parameter of paramount importance which may determine the applicability of the proposed architecture at high frequencies is the time modulation efficiency η, theoretically derived in Section 4 and specifically quantified in Section 5. The counterpart of such an efficiency in standard beamformers based on VPSs are the insertion losses. As a matter of fact, Fig. 9 plots a point cloud show-

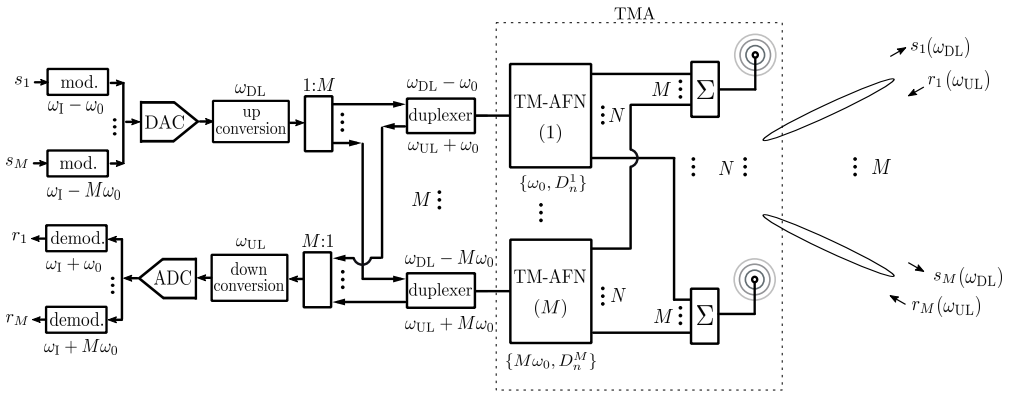

Figure 8: Proposed multibeam transceiver architecture based on TMAs with SPMT switches.

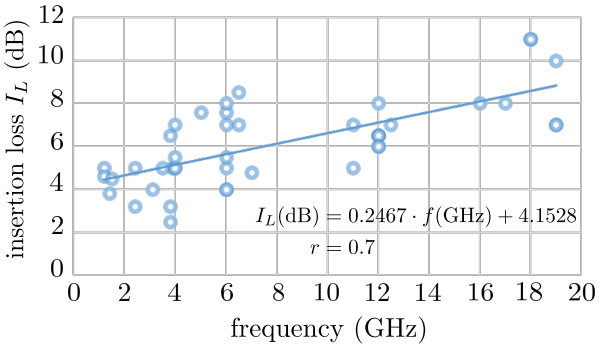

Figure 9: Insertion loss (I_L) versus frequency (bands L, S, C, X and Ku) of off-the-shelf MMIC digital phase shifters [7], [2],[4], [6], [3], [1].

ing the insertion losses of off-the-shelf MMIC digital phase shifters [1, 2, 3, 4, 6, 7] for several bands up to 20 GHz. The point cloud reveals a certain linearity (Pearson correlation coefficient $r = 0.7$) between insertion losses and frequency at these frequencies. The insertion losses (in dB) show the following statistics: range [2.5 dB, 11.0 dB], the mean value is 5.91 dB, and the standard deviation is 0.81 dB. An advantage of the TMA scheme proposed in this work is not only that the time modulation efficiency is independent of the carrier frequency, but also that shows competitive values when compared to the VPSs insertion losses.

7. Conclusion

We have presented a novel SSB TMA method, based on periodic stair-step pulses, valid for both beam-steering and beamforming purposes. The architecture is equipped with SP4T and SPST switches together with non-reconfigurable RF devices. The proposed TMA structure exhibits the following advantages: higher efficiency and flexibility, performance invariant to the carrier frequency, better cost-effectiveness, and small size. Accordingly, such a structure is particularly suitable for the design of multibeam transceivers.

Appendix A. Appendixes

Appendix A.1. Derivation of the Expression of the Sign in (3)

The Triangular numbers 1, 3, 6, 10, 15, ..., given by the formula $T_n = n(n+1)/2$, $n \in \mathbb{N}^*$, have the property that T_{4k+1} and T_{4k+2} are odd and that T_{4k+3} and T_{4k+4} are even for $k \in \mathbb{N}$. Thus, the expression

$$(-1)^{T_n} = (-1)^{\frac{n(n+1)}{2}} \tag{A.1}$$

alternates its sign according to: -1, -1, $+1$, $+1$, -1, -1, ..., and we realize that the sign behavior for $n = 1$, $n = 2$, ..., corresponds to $q = 3$, $q = 5$, ..., in the series of (3). Hence, by relating n and q through an arithmetic progression, we have that $q = 2n + 1$ or, equivalently, $n = (q-1)/2$. By substituting this expression of n in (A.1) we finally arrive at the following expression of the sign in (3):

$$(-1)^{\frac{(q+1)(q-1)}{8}}. \tag{A.2}$$

Appendix A.2. Derivation of the Sum of the Infinite Series in (26)

The polygamma function is a special function denoted by $\Psi_n(z)$ which is defined as the $(n+1)$-th

derivative of the logarithm of the gamma function $\Gamma(z)$:

$$\Psi_n(z) = \frac{d^{n+1}}{dz^{n+1}} \ln\left(\Gamma(z)\right). \tag{A.3}$$

For $n > 0$, the polygamma function can be written as [9, Chapter 6.4, pp. 260-263]

$$\Psi_n(z) = (-1)^{n+1} n! \sum_{n=0}^{\infty} \frac{1}{(z+k)^{n+1}}. \tag{A.4}$$

In particular, for $n = 1$, we have that

$$\Psi_1(z) = \sum_{n=0}^{\infty} \frac{1}{(z+k)^2}. \tag{A.5}$$

Hence, the infinite series in the expression of P_R^{TM} (26) will satisfy

$$\sum_{k=1}^{\infty} \frac{1}{(8k-7)^2} = \frac{1}{64} \sum_{k=0}^{\infty} \frac{1}{(k+1-\frac{7}{8})^2} = \frac{1}{64} \Psi_1\left(\frac{1}{8}\right), \tag{A.6}$$

and, analogously

$$\sum_{k=1}^{\infty} \frac{1}{(8k-1)^2} = \frac{1}{64} \sum_{k=0}^{\infty} \frac{1}{(k+1-\frac{1}{8})^2} = \frac{1}{64} \Psi_1\left(\frac{7}{8}\right), \tag{A.7}$$

being $\Psi_1(1/8) = 65.3881$ and $\Psi_1(7/8) = 2.0057$, and therefore, $\sum_{q \in \Upsilon} 1/q^2 = 1.053$.

References

[1] (). Aelius. `http://www.aeliussemi.com`. MMIC digital phase shifters. Accessed: 2018-08-08.

[2] (). Analog devices. `https://www.analog.com`. MMIC digital phase shifters. Accessed: 2018-08-08.

[3] (). Custom MMIC. `https://www.custommmic.com`. MMIC digital phase shifters. Accessed: 2018-08-08.

[4] (). Macom. `https://www.macom.com`. MMIC digital phase shifters. Accessed: 2018-08-08.

[5] (). Minicircuits. `http://www.minicircuits.com`. Reference: YAT series. Accessed: 2018-04-04.

[6] (). Ommic. `http://www.ommic.com`. MMIC digital phase shifters. Accessed: 2018-08-08.

[7] (). Qorvo. `http://www.qorvo.com`. MMIC digital phase shifters. Accessed: 2018-08-08.

[8] Abbosh, A. M. (2011). Broadband fixed phase shifters. *IEEE Microw. Wireless Compon. Lett.*, *21*, 22–24.

[9] Abramowitz, M., & Stegun, I. A. (1965). *Handbook of Mathematical Functions with Formulas, Graphs, and Mathematical Tables*. Dover Publications.

[10] Bogdan, G., Jarzynka, M., & Yashchyshyn, Y. (2016). Experimental study of signal reception by means of time-modulated antenna array. In *Proc. of 21st International Conference on Microwave, Radar and Wireless Communications (MIKON)* (pp. 1–4). Krakow, Poland.

[11] Bogdan, G., Yashchyshyn, Y., & Jarzynka, M. (2016). Time-modulated antenna array with lossless switching network. *IEEE Antennas Wireless Propag. Lett.*, *15*, 1827–1830.

[12] Fondevila, J., Bregains, J., Ares, F., & Moreno, E. (2004). Optimizing uniformly excited linear arrays through time modulation. *IEEE Antennas Wireless Propag. Lett.*, *3*, 298–301.

[13] Fondevila, J., Brégains, J. C., Ares, F., & Moreno, E. (2006). Application of time modulation in the synthesis of sum and difference patterns by using linear arrays. *Microw. Opt. Technol. Lett.*, *48*, 829–832.

[14] Heath, R. W., González-Prelcic, N., Rangan, S., Roh, W., & Sayeed, A. M. (2016). An overview of signal processing techniques for millimeter wave MIMO systems. *IEEE J. Sel. Topics Signal Process.*, *10*, 436–453.

[15] Hong, W., Jiang, Z. H., Yu, C., Zhou, J., Chen, P., Yu, Z., Zhang, H., Yang, B., Pang, X., Jiang, M., Cheng, Y., Al-Nuaimi, M. K. T., Zhang, Y., Chen, J., & He, S. (2017). Multibeam antenna technologies for 5G wireless communications. *IEEE Trans. Antennas Propag.*, *65*, 6231–6249.

[16] Huang, X., Guo, Y. J., & Bunton, J. D. (2010). A hybrid adaptive antenna array. *IEEE Trans. Wireless Commun.*, *9*, 1770–1779.

[17] Li, G., Yang, S., Chen, Y., & Nie, Z.-P. (2009). A novel electronic beam steering technique in time modulated antenna array. *Progress In Electromagnetics Research*, *97*, 391–405.

[18] Li, G., Yang, S., & Nie, Z. (2010). Direction of arrival estimation in time modulated linear arrays with unidirectional phase center motion. *IEEE Trans. Antennas Propag.*, *58*, 1105–1111.

[19] Maneiro-Catoira, R., Brégains, J., García-Naya, J., & Castedo, L. (2014). On the feasibility of time-modulated arrays for digital linear modulations: A theoretical analysis. *IEEE Transactions on Antennas and Propagation*, *62*, 6114–6122.

[20] Maneiro-Catoira, R., Brégains, J., García-Naya, J. A., & Castedo, L. (2017). Time modulated arrays: From their origin to their utilization in wireless communication systems. *Sensors*, *17*, 1–14.

[21] Maneiro-Catoira, R., Brégains, J., García-Naya, J. A., & Castedo, L. (2018). Analog beamforming using time-modulated arrays with digitally preprocessed rectangular sequences. *IEEE Antennas Wireless Propag. Lett.*, *17*, 497–500.

[22] Maneiro-Catoira, R., Brégains, J., García-Naya, J. A., & Castedo, L. (2018). Dual-signal transmission using RF precoding and analog beamforming with TMAs. *IEEE Communications Letters*, *22*, 1640–1643.

[23] Maneiro-Catoira, R., Brégains, J. C., García-Naya,

J. A., & Castedo, L. (2017). Enhanced time-modulated arrays for harmonic beamforming. *IEEE J. Sel. Topics Signal Process.*, *11*, 259–270.

[24] Maneiro-Catoira, R., Brégains, J. C., García-Naya, J. A., Castedo, L., Rocca, P., & Poli, L. (2017). Performance analysis of time-modulated arrays for the angle diversity reception of digital linear modulated signals. *IEEE J. Sel. Topics Signal Process.*, *11*, 247–258.

[25] Maneiro-Catoria, R., Brégains, J., Garcia-Naya, J. A., & Castedo, L. (2018). Time-modulated multibeam phased arrays with periodic Nyquist pulses. *IEEE Antennas and Wireless Propagation Letters*, *17*, 2508–2512.

[26] Maneiro-Catoria, R., Brégains, J., Garcia-Naya, J. A., & Castedo, L. (2019). Time-modulated phased array controlled with non-ideal bipolar squared periodic sequences. *IEEE Antennas and Wireless Propagation Letters*, *18*, 407–411.

[27] Méndez-Rial, R., Rusu, C., González-Prelcic, N., Alkhateeb, A., & Heath, R. W. (2016). Hybrid MIMO architectures for millimeter wave communications: Phase shifters or switches? *IEEE Access*, *4*, 247–267.

[28] Poli, L., Moriyama, T., & Rocca, P. (2014). Pulse splitting for harmonic beamforming in time-modulated linear arrays. *International Journal of Antennas and Propagation*, *1*, 1–9.

[29] Poli, L., Rocca, P., Oliveri, G., & Massa, A. (2011). Harmonic beamforming in time-modulated linear arrays. *IEEE Trans. Antennas Propag.*, *59*, 2538–2545.

[30] Rocca, P., Zhu, Q., Bekele, E., Yang, S., & Massa, A. (2014). 4-D arrays as enabling technology for cognitive radio systems. *IEEE Trans. Antennas Propag.*, *62*, 1102–1116.

[31] Shanks, H. (1961). A new technique for electronic scanning. *IRE Transactions on Antennas and Propagation*, *9*, 162–166.

[32] Tong, Y., & Tennant, A. (2010). Simultaneous control of sidelobe level and harmonic beam steering in time-modulated linear arrays. *Electronics Letters*, *46*, 201–202.

[33] Tong, Y., & Tennant, A. (2012). A two-channel time modulated linear array with adaptive beamforming. *IEEE Trans. Antennas Propag.*, *60*, 141–147.

[34] Yao, A. M., Wu, W., & Fang, D. G. (2015). Single-sideband time-modulated phased array. *IEEE Trans. Antennas Propag.*, *63*, 1957–1968.